A high-resolution small animal SPECT system developed at Tsinghua

DAI Tiantian MA Tianyu* LIU Hui CUI Junjian WEI Qingyang
LIU Yaqiang WANG Shi

Key Laboratory of Particle & Radiation Imaging, Ministry of Education; Department of Engineering Physics, Tsinghua University, Beijing 10084, China

Abstract An SPECT system dedicated to small animal imaging shall be of a millimeter spatial resolution or even better. This study was aimed at achieving 0.5-mm spatial resolution for a small animal SPECT system at low cost. It was developed from a single-head clinical SPECT scanner, with a seven-pinhole collimator and a four-degree-of-freedom motion control stage. Several key techniques were developed, including high-resolution image reconstruction algorithm, high accuracy geometrical calibration method, and optimized system matrix derivation scheme. The system matrix was derived from Monte-Carlo simulation and de-noised by fitting each point spread function to a two dimensional Gaussian function. Experiments of point source and ultra micro hot rod phantom were conducted. With a spatial resolution of 0.5–0.6 mm, this system provides a practical way for low-cost high-resolution animal imaging on a clinic SPECT system.

Key words SPECT, Multi-pinhole collimator, High resolution, System matrix, Image reconstruction

1 Introduction

Small animal imaging has become increasingly popular in molecular imaging in recent years, as an irreplaceable tool in preclinical researches and biomedical studies[1]. On a small animal SPECT, 3D functional imaging can be performed to determine not only the location and size of cancer lesions but also the functionality and malignancy of the lesions, especially for myocardium lesions, thyroid, bone, etc[2]. A major challenge of small animal imaging is to do it in high spatial resolution (≤1 mm) in a small field of view (FOV), e.g. a 30-mm cross-section of a mouse. Several approaches were implemented in animal SPECT systems[2–6], which achieved remarkably. Using high intrinsic spatial resolution detector[3,4], some dedicated systems achieved sub-millimeter resolution, though the high cost limited their applications in small animal imaging. Some groups combined clinical SPECT scanners with dedicated high-resolution collimators (e.g. pinhole[5,6] and slit-slat[7] collimators). Having larger size detectors (typically 300–500mm), hence a larger magnification factor, a clinical SPECT may achieve high spatial resolution, reportedly 0.6–0.7 mm [8], with less cost than a dedicated system.

In many small animal SPECT systems, pinhole collimation is used to achieve high spatial resolution thanks to zoomed projections[3,5,6,9]. However, a pinhole is in diameter of sub-millimeter to several millimeters, hence a much lower detection sensitivity of a single pinhole SPECT system than a clinical SPECT, while using multi-pinhole collimators to improve the detection sensitivity to a reasonable level shall bring new challenges in pinhole design, geometrical calibration and image reconstruction.

Iterative image reconstruction algorithms are widely used in multi-pinhole SPECT. To achieve high spatial resolution, an accurate system model is required for the geometry and photon physics effects, and the modeling accuracy can be evaluated by measurement[10] and analytical[11,12] methods, or Monte Carlo simulation[13,14]. The measurement method can be done on the entire system matrix over the whole

Supported by Specialized Research Fund for the Doctoral Program of Higher Education (SRFDP200800031071), National Natural Science Foundation of China (No.10975086), and the National High Technology Research and Development Program of China (No. 2006AA020802).

* Corresponding author. *E-mail address*: maty@tsinghua.edu.cn

Received date: 2011-04-25

FOV in one single run, accounting for various physical and geometrical factors with high accuracy, with tremendous acquisition time, though. Analytical calculation is fast, but a simplified projection model differs in any way from an actual system. M-C simulation method, however, can model more detailed geometry of collimator and scanner settings, and physical process of the animal SPECT system, at a cost of intensive computational burden.

In this paper, a multi-pinhole collimator scheme is designed for animal SPECT imaging. Several techniques were used to obtain accuracy of the optimized system matrix and SPECT image quality. Geometric parameters were determined by point source measurement and accurate calibration procedure, and the system matrix was derived from M-C simulation, in which both the system geometry and photon interaction physics were modeled, and the system matrix is de-noised by fitting each PSF to a 2D Gaussian function. To evaluate performance of the proposed method, experiments were done with a dual-point-source phantom and a micro hot rod phantom.

2 Materials and Methods

2.1 The experimental animal SPECT system

The small animal SPECT was based on a Hamamatsu BHP6601 SPECT scanner. It has a single monolithic NaI(Tl) detector with effective detection area of 510 mm × 390 mm, and 9.5-mm thickness, with an intrinsic spatial resolution of R_i = 3.55 mm (FWHM) and an energy resolution of 9.9% @140 keV(^{99m}Tc). In order to perform small animal imaging, the original parallel-hole collimator was removed, and a seven-pinhole collimator and a four-degree-of-freedom (4-DOF) motion control stage are placed under the SPECT detector (Fig.1). The collimator consists of a tungsten slab and multiple tungsten pinhole-inserts.

With a changeable pinhole insert, the design provides a flexible way for performing small animal imaging on a clinical SPECT system. The animal scanning bed fixed to the 4-DOF motion control stage can be moved in three orthogonal translational directions, and rotated around the body axis with positioning precision of 3–5 μm. Pinhole diameters, opening angle, etc can be optimized towards different application purposes. For achieving a 0.5-mm spatial resolution of the system, a seven-pinhole collimator was designed with *Φ*0.4 mm knife-edge pinhole inserts of 40° opening angle. Details of the imaging performance criteria and parameter optimization, and comparisons between the single- and seven-pinhole collimator designs, can be found in Ref.[15].

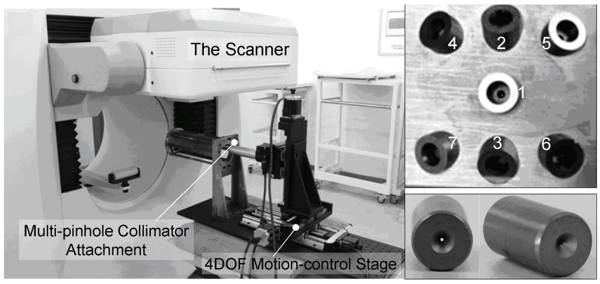

Fig.1 The small animal SPECT system and its collimator slab with seven pinhole inserts (the right).

2.2 Geometrical calibration

A small error in estimating the system geometric parameters, e.g. the location of each pinhole, may well be magnified through pinhole imaging process and result in severe resolution loss in image reconstruction. Therefore, geometrical parameters of the experimental system were determined by an accurate calibration procedure. A *Φ*0.5 mm point source was fixed to the animal bed, and moved by a certain scanning path, encompassing three circular orbits around the long axis of the bed. The rotation radii of the three orbits were the same, and the rotation center of one orbit was 4.5 mm apart from its adjacent orbit. In each orbit, the point source was rotated in 180 2º-steps. After each rotation, one frame of SPECT projection data was acquired for 5 s, and the data were processed to identify the point source projection corresponding to each pinhole. Finally, the mass-coordinate centers of the point source projection were calculated from the projection image.

The calibration included 28 geometrical parameters: 3 Cartesian coordinates of the seven pinhole centers, the 3 Cartesian coordinates of the detector center, the tilt and twist angles of detector plane, the radius-of-rotation of the point source, and the initial acquisition angle of the point source. A geometrical projection equation was derived, and it was used to calculate the projection centers of the point sources and a specific set of system parameter. The calibration parameters underwent a non-linear least-square fitting procedure[16], in which the parameters were updated iteratively by comparing the projection centers calculated from the geometrical projection equation to the measured ones. Accuracy of the calibration was evaluated by an SVD (Singular Value Decomposition) -based method proposed in Ref. [17]. By analyzing standard derivation of the estimated parameters, the calibration precisions were 0.01 mm and 0.01 rad, which are is sufficient to achieve the 0.5-mm spatial resolution.

2.3 System matrix derivation

The iterative algorithm of ordered subset expectation maximization (OSEM) was chosen to reconstruct image from the simulation results. The iterative update equation is[18, 19]

$$f_{si}^{q+1} = \frac{f_{si}^{\ q}}{\sum_{j\in S_q} c_{ij}} \sum_{j\in S_q} \frac{c_{ij} p_j}{\sum_{i'} c_{i'j} f_{si'}^{\ q}} \tag{1}$$

where, p_j is the j^{th} measured projection, and projections are divided into L subsets $\{S_q\} = \{S_1, S_2\ldots, S_L\}$; $f_{si}^{\ q}$ is the estimated activity of i^{th} pixel after the q^{th} sub-iteration in s^{th} iteration; the operator $\sum_{j\in Sq}\cdot$ represents the sum of all the projection belonging to subset S_q, and c_{ij} is the contribution of the i^{th} pixel to the j^{th} projection.

The ensemble of $\{c_{ij}\}$ is defined as the system matrix. When the updated image $f_{si}^{\ q}$ approaches the true image, an accurate system matrix guarantees that the estimated projection $\sum_{i'} c_{i'j}\, f_{si'}^{\ q}$ is close to the measured projection (p_j), and the iteration is converged to the true solution. Therefore, accuracy of the system matrix is a critical factor to obtain high quality image.

An accurate system matrix should model precise geometry and physical photon interaction process. After the calibration process, the following steps were performed to derive an accurate system matrix:

(1) Calculation of each PSF(point spread function) center. For each voxel in the FOV, the PSF center is defined as the point where the line connecting the voxel and center of certain pinhole aperture intersects the detector plane. The PSF center coordinates for each pinhole were calculated, and a look-up table was pre-stored.

(2) Size optimization of the system matrix. The voxel size in the image space was chosen as 0.45 mm ×0.45 mm×0.5 mm; and the pixel size in the detector plane, as 2.0 mm×2.0 mm; and the system matrix size, as 9×9, to ensure that the most of detected events fall into the limited area.

(3) The simulation package of GATE v6.0.0[20] was used to model the SPECT system with calibrated geometry. A uniform cylindrical source filling the entire FOV was specified, with an activity of 2 mCi. The acquisition time was 47 607 s. Photon events of 1.77×10^8 were collected and stored in a ROOT-format[21] list-mode data file.

(4) In the system matrix, each element represents the number of events emitted from a certain position and detected in a certain position of the detector, and the positions had been recorded in the list-mode data file. The simulated events were read one-by-one from the list-mode data file by a derivation program, and histogramed into the corresponding element of the system matrix by its emission and detection positions.

(5) In order to reduce the statistical noise in the system matrix, a PSF-denoising procedure is performed by a 2-D Gaussian function,

$$f(x,y)=c\exp[a_1(x-x_0)^2+2a_2(x-x_0)(y-y_0)+a_3(y-y_0)]^2 \tag{2}$$

Fig. 2(a) and 2(b) are PSFs before and after 2-D Gaussian fitting, and in Fig.2(c) the horizontal profiles of both PSFs are compared. To validate efficacy of the proposed M-C-based PSF-derivation process, a system matrix modeling just the system geometry, i.e. a geometry-only system matrix, was assumed, with pinholes being ideal and all events being deposited in the center of PSF, and the results are shown in Fig.2(d).

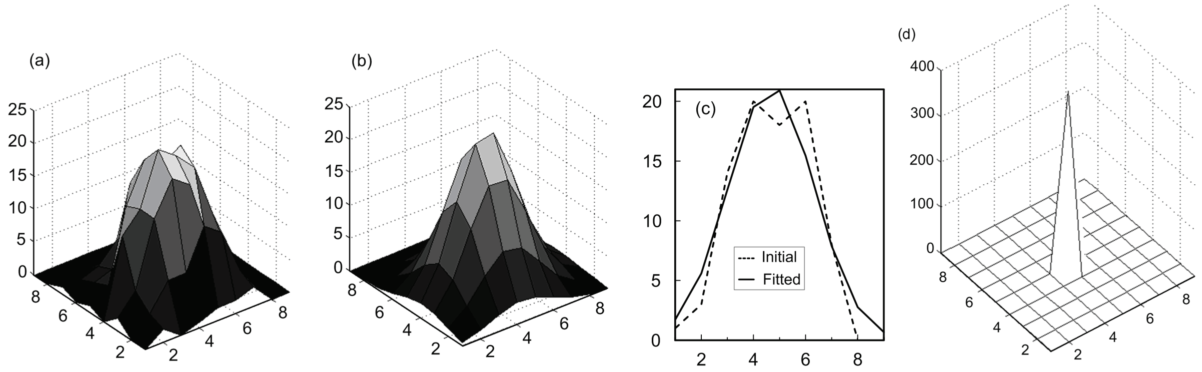

Fig.2 PSFs from the M-C simulation (a), after 2-D Gaussian fitting (b), the horizontal profile of both PSFs (c), and the PSF of geometry-only system matrix for the same voxel and pinhole.

2.4 Point source/phantom experiments and image reconstruction

The spatial resolution was evaluated with a phantom consisting two *Φ*0.5 mm ^{99m}Tc point sources of 0.45 mCi each. The phantom were placed about 6 mm off the center of FOV, and the edge-to-edge distance between the two point sources was 0.5 mm. The point sources were rotated in 180 2°-steps, and SPECT projection data were acquired for 15 min. The dual-point-source projections in one rotational step are shown in Fig.3.

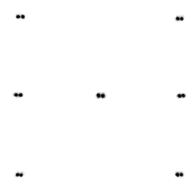

Fig.3 One acquired projection of a dual-point-source phantom with 0.5 mm edge-to-edge distance.

The acquired data were used for image reconstruction with an OSEM iterative program. Critical reconstruction parameters, such as optimal number of ordered subsets and iterations, and image voxel size, were empirically chosen to reach a balance between image resolution and noise. Two cases with fitted and non-fitted system matrix were compared, and their dual-point-source reconstructed images are shown in Section 3.1.

The spatial resolution was evaluated with a micro hot rod phantom having six hot-rods in diameters of 0.5, 0.6, 0.75, 1.0, 1.2, and 1.5 mm. Center-to-center distance between adjacent hot rods was twice as long as the diameter. ^{99m}Tc solution of 1.7 mCi was filled in the hot-rod sections, with the phantom activity being 8.5 mCi. The phantom was scanned by a circular orbit (180 steps and 2° per step), and data were acquired for 1.5 h.

Both cases were reconstructed using geometry -plus-physics matrix and geometry-only system matrix. Iterated by OSEM program, the reconstructed phantom images are shown in Section 3.2.

3 Results

3.1 Point source studies

Transaxial slices and profiles of the reconstructed images (4 iterations, 18 subsets) of the dual-point - source phantom are shown in Fig.4, indicating the image reconstructed by system matrices before and after PSF fitting. Voxel size in point source reconstruction was 0.15 mm×0.15 mm×0.15 mm, the two point sources can promisingly be separated in the case of 0.5 mm edge-to-edge distance. The fitted PSF provides slightly better peak-to-valley ratio in the profile, resulting in a little improvement in spatial resolution.

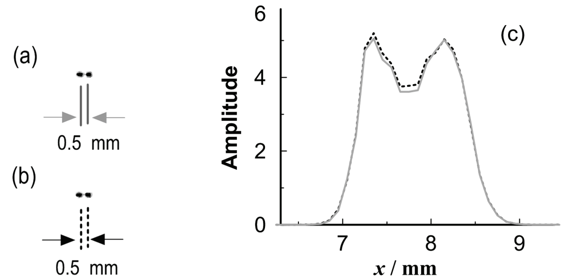

Fig.4 Reconstructed transaxial-slice images of the dual-point -source (0.5 mm edge-to-edge distance) with (a) and without (b) PSF fitting, and profile of the reconstructed images (c).

3.2 Ultra micro hot rod phantom study

Figure 5(a) shows the reconstructed images of the ultra micro hot rod phantom with Monte-Carlo-based geometry-plus-physics system matrix (20 iterations, 20 subsets). 30 slices (15 mm thick) are summed together to reduce noise, and voxel size in hot rod phantom reconstruction was 0.1125 mm×0.1125 mm×0.5 mm. All hot rods of 0.6 mm diameter are identifiable clearly. Fig.5(b) shows the reconstructed images of the same phantom with geometry-only system matrix in the reconstruction, indicating that the geometry-plus-physics system matrix can provide more accurate modeling of the system, and the Monte-Carlo-based PSF derivation method can achieve good resolution recovery.

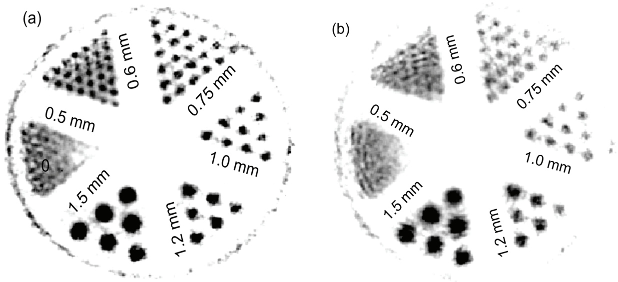

Fig.5 Reconstructed transaxial images of the phantom with hot rods in diameters of 0.5, 0.6, 0.75, 1.0, 1.2 and 1.5 mm. (a) with Monte-Carlo-based geometry-plus-physics system matrix, (b) with geometry-only system matrix.

4 Conclusions

We have developed a prototype animal SPECT system based on a clinical SPECT detector and an add-on multi-pinhole collimator. The highly flexible design makes the collimator easily adaptable to various existing clinical SPECT systems and for different application purposes. A seven-pinhole collimator is manufactured; high accuracy calibration techniques and system matrix derivation methods based on Monte Carlo simulations are discussed. Improved image quality is observed with a post-denoising step on the generated system matrix. The results about point sources and ultra micro hot rod phantoms demonstrate that 0.5–0.6 mm image resolution is achievable. The proposed technology is attractable for its high feasibility and reproducibility.

References

1 Chatziioannou A F. Proc Am Thorac Soc, 2005, **2:** 533–536.
2 Meikle S R, Kench P, Kassiou M, *et al*. Phys Med Biol, 2005, **50:** R45–R61.
3 Beekman F J, Vastenhouw B. Phys Med Biol, 2004, **49:** 4579–4592.
4 Kastis G A, Barber H B, Barrett H H, *et al*. IEEE Trans Nucl Sci, 2000, **47:** 1923–1927.
5 Beekman F J, van der Have F, Vastenhouw B, *et al*. J Nucl Med, 2005, **46:** 1194–1200.
6 Schramm N U, Ebel G, Engeland U, *et al*. IEEE Trans Nucl Sci, 2003, **50:** 315–320.
7 Shao Y, Ma T, Yao R. IEEE Nucl Sci Symp Conf Rec, 2007, 4285–4288.
8 DiFilippo F P. Phys Med Biol, 2008, **53:** 4185–4201.
9 Dai Q, Qi Y. At Energ Sci Technol, 2009, **43:** 1034–1038.
10 Rowe R K, Aarsvold J N, Barrett H H, *et al*. J Nucl Med, 1993, **34:** 474–480.
11 Metzler S D, Bowsher J E, Greer K L, *et al*. IEEE Trans Med Imag, 2002, **21:** 878–886.
12 Bal G, Acton P D. Phys Med Biol, 2006, **51:** 4923–4950.
13 Refecas M, Mosler B, Dietz M, *et al*. IEEE Trans Nucl Sci, 2004, **51:** 2597–2605.
14 Yao R, Ma T, Shao Y. IEEE Trans Nucl Sci, 2009, **56:** 2651–2658.
15 Dai T, Liu Y, Ma T, *et al*. At Energ Sci Technol, 2011, **45:** 369–373.
16 Liu H, Ma T, Dai T, *et al*. **M18-224:** High accuracy geometrical calibration for half-mm animal SPECT imaging. IEEE NSS MIC RTSD, Knoxville, Tennessee, Oct, 2010.
17 Ma T, Yao R, Shao Y, *et al*. IEEE Trans Med Imag, 2009, **28:** 1929–1939.
18 Shepp L A, Vardi Y. IEEE Trans Med Imag, 1982, **MI-1:** 113–122.
19 Hudson H M, Larkin R S. IEEE Trans Med Imag, 1994, **12:** 601–609.
20 Jan S, Santin G, Strul D, *et al*. Phys Med Biol, 2004, **49:** 4543–4561.
21 Brun R, Rademakers F. Nucl Inst Meth Phys Res A, 1997, **389:** 81–86. See also http://root.cern.ch/.